Anisotropy and orbital moment in Sm-Co permanent magnets

Bhaskar Das, Renu Choudhary, Ralph Skomski, Balamurugan Balasubramanian, Arjun K. Pathak, Durga Paudyal, and David J. Sellmyer

Phys. Rev. B **100**, 024419 — Published 18 July 2019

DOI: 10.1103/PhysRevB.100.024419

Anisotropy and Orbital Moment in Sm-Co Permanent Magnets

Bhaskar Das,[1,2] Renu Choudhary,[2] Ralph Skomski,[1] Balamurugan Balasubramanian,[1] Arjun K. Pathak,[2] Durga Paudyal,[2] and David J. Sellmyer[1]

[1]*Nebraska Center for Materials and Nanoscience and Department of Physics and Astronomy University of Nebraska, Lincoln, NE 68588*

[2]*Ames Laboratory, U.S. Department of Energy, Iowa State University, Ames, IA 50011*

Abstract

Structural and magnetic properties of iron-free and iron-substituted $SmCo_5$ have been investigated theoretically and experimentally. The nanocrystalline ribbons, which were produced by rapid solidification, $SmCo_{5-x}Fe_x$ ($0 \leq x \leq 2$) crystallize in the hexagonal $CaCu_5$ structure for $x \leq 0.75$. Small Fe additions ($x = 0.25$) substantially improve the coercivity, from 0.45 T to 2.70 T, which we interpret as combined intrinsic and extrinsic effect. Most of our findings are consistent with past samarium-cobalt research, but some are at odds with findings that have seemingly been well-established through decades of rare-earth transition metal research. In particular, our local spin density approximation with Hubbard parameter (LSDA+*U*) calculations indicate that the electronic structure of the Sm atoms violates Hund's rules and that the orbital moment is strongly quenched. Possible reasons for the apparent disagreement between theory and experiment are discussed. We explicitly determine the dependence of the Sm 4*f* charge distribution, arguing that an accurate density-functional description of $SmCo_5$ is a challenge to future research.

I. INTRODUCTION

Samarium-cobalt alloys are a fascinating class of magnetic materials that have played an important role in permanent magnetism and modern technology [1-9]. They were the first high-performance rare-earth permanent magnets [1,3,10] and dominate in high-temperature high-energy-product applications even today [8,11,12]. The development started with $SmCo_5$, which combines a relatively high saturation magnetization M_s and a high Curie temperature T_c with an excellent magnetocrystalline anisotropy constant K_1 of about 17.2 MJ/m^3 [1,2,7,13,14]. However, Sm and Co are fairly expensive elements, and atomic substitutions began to be explored around 1970 [13,15,16,17].

The original focus was on replacing Co by Fe, with the aim at simultaneous reducing the raw-materials price and further improving the magnetic properties, especially the magnetization. An obstacle is the very limited equilibrium solubility of Fe in the $SmCo_5$ phase, which is metastable even without Fe addition. Other additives, such as Ti, Cu, Zr, Nb, and Ni, which were also considered from a very early stage [5,16,17,18,19,20-26], often improve coercivity but tend to further reduce the magnetization and can therefore only be used in small amounts. A

breakthrough occurred with the recognition that Co-doping with Cu enhances the solubility of Fe and eventually leads to the formation of a high-magnetization $Sm_2(Co_{1-x}Fe_x)_{17}$ phase surrounded by $Sm(Co, Cu)_5$ grain boundaries [3,16,27,28]. The anisotropy of Sm_2Co_{17} is lower than that of $SmCo_5$ by a factor of about 4, but the cellular microstructure of the 2:17 magnets is ideal for coercivity development [5, 12, 28-34]. Without the addition of Cu, the amount of Fe in $SmCo_5$ can be enhanced by rapid quenching from the melt, because the Fe solubility in $SmCo_5$ increases with temperature [18, 35, 36]. The practical disadvantage of this approach is the low remanence ratio of these essentially isotropic magnets, which overcompensates the magnetization gain due to iron addition, putting them at a competitive disadvantage compared to sintered Sm_2Co_{17} magnets. In fact, it was recently suggested [26] that the addition of Ni in Fe substituted $SmCo_5$ stabilizes the 1:5 structure by adding 3*d* electrons.

The magnetic properties of rare-earth transition metal (RE-TM) intermetallic alloys are well understood from the viewpoint of individual atomic contributions. Soon after the discovery of $SmCo_5$, it was recognized that the crystal-field interaction of the Sm^{3+} ion in the hexagonal crystal field is the main reason for the high anisotropy of $SmCo_5$ and of related intermetallics [6,17,37-40]. Early experimental and theoretical work on the topic was reviewed in the 1970s by Buschow [17] and by Kirchmayr and Poldy [38]. Since then, much progress has been made in the theoretical description of the transition-metal sublattice [41-43], and this trend includes the LSDA+*U* calculations.

Figure 1 shows the crystal structure of the hexagonal intermetallic compounds $SmCo_5$ (prototype $CaCu_5$), which consists of alternating Co and Sm-Co layers. Experiment and model calculations show that the alloy's intrinsic properties (magnetization, Curie temperature, anisotropy) reflect the existence of RE (1a) and TM (2c, 3g) sublattices coupled by moderately strong intersublattice exchange [6,17,37-39,44-46]. The RE moments are predominantly of localized 4*f* character and supposed to obey Hund's rules, whereas the TM sublattice magnetization is of the itinerant 3*d* type. The two-sublattice picture and the Hund's-rule character of the rare-earth magnetism are strongly supported by a broad range of experiments, including the temperature dependence of intrinsic properties and rare-earth spectroscopy [47]. For example, comparison of R_xT_y intermetallics (T = Fe, Co) having magnetic and nonmagnetic rare earth R makes it possible to separate RE and TM contributions to magnetization, Curie-temperature, and anisotropy [6,17,38,44,45]. This approach has been followed by researchers from decades in permanent magnetism, including 1:5 magnets [6, 15, 17, 38].

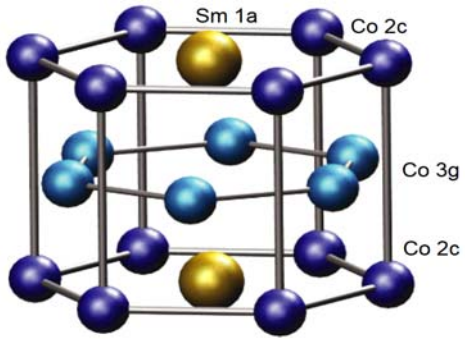

FIG. 1. A unit cell of the hexagonal intermetallic $SmCo_5$.

Given the huge amount of past work on partially substituted Sm-Co, it is surprising how little has been published about $Sm(Co, Fe)_5$. There are several reasons. On the experimental side, accurate measurements are difficult to perform due to the very high anisotropy field $H_a = 2 K_1/\mu_o M_s$ of $SmCo_5$ and due to the metastability of $SmCo_5$ and $SmCo_{5-x}Fe_x$. Iron has long been added in various amounts to commercial Sm-Co magnets, and there is a strong incentive to avoid the dissemination of the corresponding information.

The theoretical problems are more scientific. The transition-metal sublattice is well understood through LSDA density functional theory (DFT) calculations [41-43,48], including the approach used in the present paper. These calculations have supplanted and improved earlier semiquantitative approaches, based for example on the Stoner theory [17,38]. The same arguments apply to the nonmagnetic rare earth elements Y, La, and Lu.

By contrast, magnetic rare-earth atoms in RE-TM intermetallics are much less well-described from first principles, due to strong Hund's-rules correlations in the localized 4*f* shells, and the traditional crystal-field model has remained superior in the description of rare-earth sublattice at both zero and finite temperatures [6,17,38,49]. With a few exceptions, such as Ce-containing heavy-fermion compounds, the rare-earth 4*f* electrons are localized [50-52], whereas the LSDA is intrinsically delocalized. The LSDA+*U* improves the predictions of the LSDA, but only selectively. It provides corrections to physical properties such as charge state (tripositive in the case of Sm), spin moment, orbital moment, anisotropy, and splittings of term, multiplet, and intramultiplet energy levels. There is, however, no reason to believe that a single parameter (*U*) or two strongly coupled intra-atomic parameters (*U* and *J*) provide a simultaneous description of all properties, as required for the understanding of magnetocrystalline anisotropy. There are also qualitative shortcomings. For example, both experiment and highly accurate many-electron calculations reveal central peaks around the Fermi level of materials near metal-insulator transitions [52], and these peaks are not reproduced by LSDA+*U*. The central peak arises from many-electron quantum fluctuations and indicates the limited applicability of the LSDA+U. Highly correlated 4f electrons make the first-principles approach complex and difficult [53]. In fact, the localized character of the 4*f* electrons means that Sm is on the 'wrong' side of the aisle from the viewpoint of one-electron theory.

In this paper, we have experiment and DFT calculations to investigate the structural stability, magnetization, and anisotropy of $SmCo_{5-x}Fe_x$. Our LSDA+*U* calculations yield a strong degree of orbital-moment quenching, which amounts to a violation of Hund's rules and is contradictory to the seemingly well-established two-sublattice picture of RE-TM (Sect. II). The problem is rationalized in real space by plotting 4*f* charge density as a function of the magnetization angle, showing how the net interatomic hybridization between TM 3*d* and RE 4*f* electrons leads to a possibly overestimate quenching (Sect. III).

II. METHODS AND RESULTS

Experimentally, stoichiometric amounts of high purity Sm, Fe, and Co elements were arc-melted in an argon atmosphere. The melting was done repeatedly (at least 5 times) to get homogeneously mixed ingots. The weight loss after melting was less than 0.5% in each composition of $SmCo_{5-x}Fe_x$ ($0 \leq x \leq 2$). The arc-melted ingots were then used to produce melt-spun ribbons, using a copper wheel kept at room temperature and rotating at a speed of 22 m/s.

The compositions of the samples were confirmed using energy dispersive x-ray spectroscopy (EDX) attached to a JEOL JSM 840A scanning electron microscope.

The melt-spun ribbons were mechanically milled to fine-grained powder for X-Ray diffraction (XRD, Rigaku D/Max-B x-ray diffractometer) studies, where a *Cu* K_α wavelength of 1.54 Å was used. The X-ray diffraction (XRD) patterns of the powdered $SmCo_{5-x}Fe_x$ samples (Fig. 2) confirm the hexagonal $CaCu_5$-type structure for $x \leq 0.75$. In the expanded XRD, Fig. 2(b), the shift in the peak positions upon Fe addition, especially that of the (110) and (101) peaks (dotted lines), is due to the lattice expansion caused by the replacement of Co by Fe [54]. This expansion is also evident from the change in the lattice parameters (with uncertainties ≤ 0.05 %) *c*, 3.987 Å, 4.014 Å, and 4.020 Å, and *a*, 4.979 Å, 4.985 Å, and 4.993 Å for $x = 0$, 0.5 and 0.75, respectively. The average grain size of the ribbons lies in the range 30 – 50 nm, which was determined using the Scherrer formula on the prominent peaks (200) and (111) in the powder x-ray diffraction patterns and an average value was taken [55,56]. The ribbons were ground into fine powders by mechanical milling and therefore the shape of the grains is considered spherical and subsequently used a standard K = 0.9 in Scherrer formula [55,56]. Figure 2c shows a mixture of $SmCo_5$ and Sm_2Co_{17} phases.

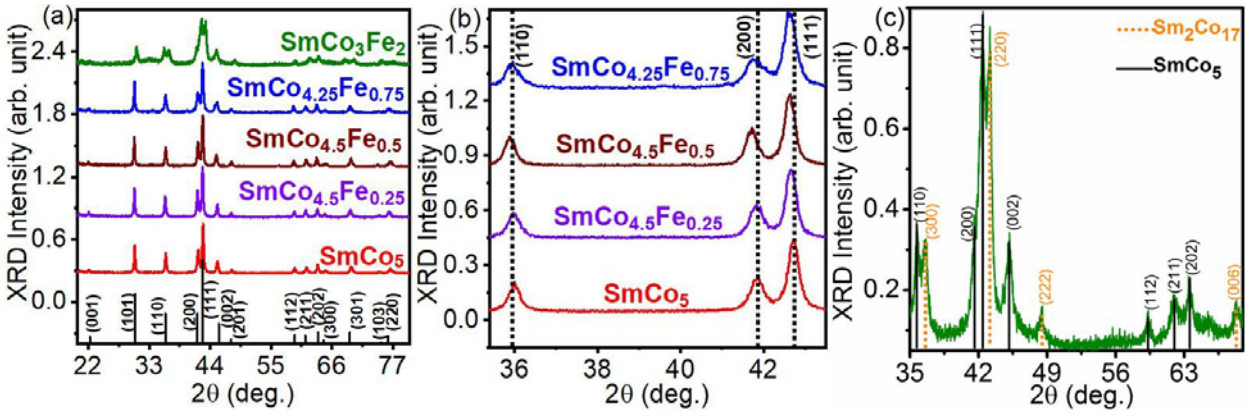

FIG. 2. X-ray diffraction (XRD) analysis of $SmCo_{5-x}Fe_x$: (a) patterns for $x = 0$, 0.25, 0.5, 0.75 and 2 compared with the prototype $CaCu_5$-structure (vertical lines), (b) expanded view showing peak-shift towards lower angles due to Fe addition (vertical dotted lines), and (c) $SmCo_3Fe_2$ showing mixture of $SmCo_5$ (vertical solid lines) and Sm_2Co_{17} (vertical dotted lines).

The room temperature field dependence of the ribbons' magnetization was measured using a superconducting quantum interference device (SQUID). For this, the ribbons were placed inside a gelatin capsule, placed in the middle of a straw, and loaded in the SQUID for the magnetic measurements. This is the most common procedure used for measuring powder samples. Both capsule and straw, provided by Quantum Design, are diamagnetic. The diamagnetic signal of the capsule and straw was measured and corrected. Figure 3(a) compares the room-temperature hysteresis loops of the $SmCo_5$ and $SmCo_{4.75}Fe_{0.25}$: the coercivity increases from 4.5 kOe ($SmCo_5$) to 27 kOe ($SmCo_{4.75}Fe_{0.25}$). For $x = 2$, the wasp-taille room-temperature hysteresis loop (Fig. 3b) indicates a mixture of 1:5 and 2:17 phases, in accordance with the XRD measurements. Figure 4 summarizes the magnetic properties of $SmCo_{5-x}Fe_x$ for $0 \leq x \leq 2$. Here, J_s is the saturation magnetic polarization which is the calculated value of the quantity $4\pi M_s$

where M_s is the saturation magnetization (in emu/cm^3). Note that, since the hysteresis loops are not saturating at high field (70 kOe), the magnetization values at the highest available field (70 kOe) are taken as the M_s values for this calculation considering the nominal density of the samples. The large coercivity increase between $x = 0$ and $x = 0.25$ is indicative of an enhanced anisotropy constant, although microstructural changes also play a role. Note that, the difference in the values of H_c mentioned in this report to the other related work is minimal and is due to the variation in several experimental factors such as wheel speeds, crystallite grain sizes and stability of the $SmCo_5$ phase at different conditions. [25,36]

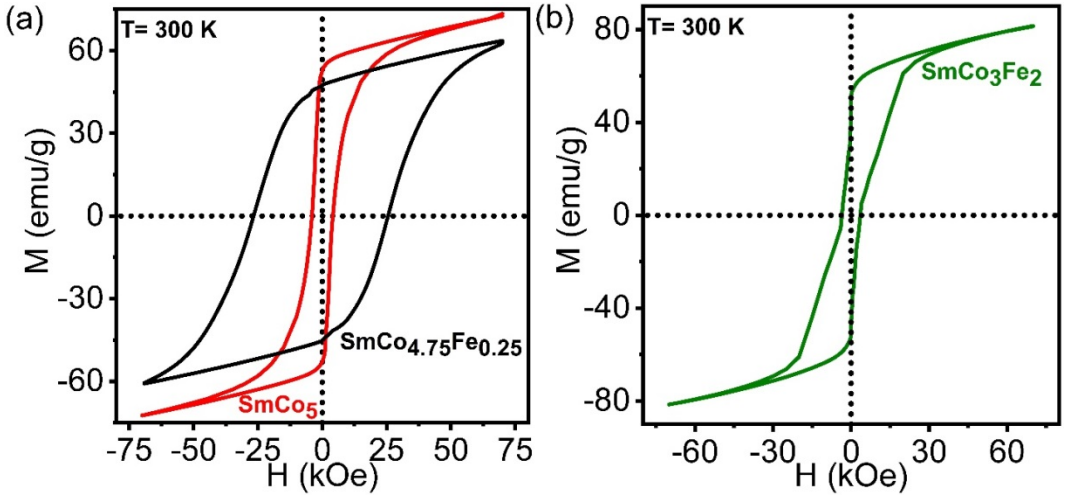

FIG. 3. Hysteresis loops: (a) comparison of $SmCo_5$ and $SmCo_{4.75}Fe_{0.25}$ and (b) two-phase loop $SmCo_3Fe_2$ exhibiting a hard-soft two-phase characteristic.

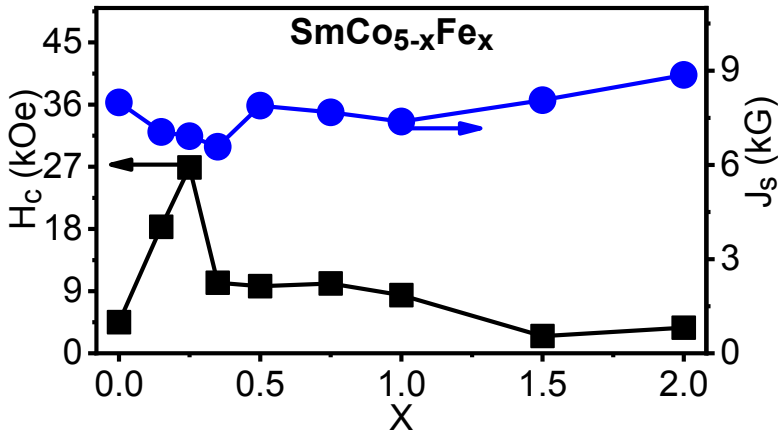

FIG. 4. Coercivity H_c and magnetization (polarization J_s) of $SmCo_{5-x}Fe_x$ as a function of Fe content.

To calculate the phase stability, electronic structure, magnetization, and magnetocrystalline anisotropy of pure and Fe substituted $SmCo_5$, we have employed the local spin-density approximation including onsite electron correlation (LSDA+U) and spin-orbit coupling (SOC) within the framework of full potential linearized augmented plane wave (FP-LAPW) method [14]. The k-space integration used as Brillouin-zone mesh of at least 16 × 16 × 16, which was sufficient for the convergence of total energies (10^{-7} Ry), charges, and

magnetic moments. For the FP-LAPW, the cutoff parameters RK_{max} and G_{max} were 9 and 16, respectively. We set the cutoff between core and valence states to -6.0 Ry.

The dashed-dotted green curve in Fig. 5 shows the formation energy of $SmCo_{5-x}Fe_x$ calculated as a function of the iron content x; negative values of the formation energy indicate that phase formation is energetically favorable. The curve shows that $SmCo_{5-x}Fe_x$ is stable for up to $x \leq 1$ but unstable for $x \geq 2$. This trend agrees with the past and present experimental findings outlined above. Note, however, that the formation energy is only partially indicative of the structural stability of $SmCo_{5-x}Fe_x$ because it considers the stability of the phase with respect to the elements Sm, Co, and Fe. The experiment shows that the structural competition is not between the 1:5 phase and the elements but involves the 1:5 and 2:17 phases. A full structural-stability analysis would require the inclusion of $Sm_2Co_{17-y}Fe_y$ and other phases, which we have not attempted.

The magnetocrystalline anisotropy energy (MAE) was obtained as the total energy difference between moment alignment in the a-b basal plane and in the c-direction. Positive MAE indicates easy-axis anisotropy ($K_1 > 0$) and negative MAE indicates easy-plane anisotropy ($K_1 < 0$). In order to test the influence of the onsite electron correlation of the Sm atoms on the anisotropy, we have considered different values of $U - J = 4$ to 6.7 eV. The calculated anisotropy values of $SmCo_5$ are 11.2 meV/f.u. (18 MJ/m^3) for $U - J = 6.0$ eV and 8.8 meV/f.u. (14 MJ/m^3) for $U - J = 6.7$ eV. These results are in fair agreement with the experimental zero-temperature anisotropy of about 30 MJ/m^3 [38]. In the following, we use $U - J = 6.0$ eV for all remaining calculations. The dashed red line in Fig. 5 shows the calculated magnetocrystalline anisotropy as a function of iron content. Our anisotropy predictions qualitatively agree with past DFT calculations on $SmCo_{5-x}Fe_x$ [41], except for a slight anisotropy increase for very small Fe contents ($x < 0.15$), which may be due to the use of the virtual-crystal approximation (VCA) for this range in Ref. 41. Between $x = 0.15$ and $x = 0.25$, both the present anisotropy calculations and those of Ref. 41 contradict our experimental conclusions drawn from Figs. 3-4. For large Fe contents, all experimental and theoretical results indicate a decrease of K_1 with increasing x. The shallow anisotropy minimum at $x = 1$, which was also found in Ref. 41, is consistent with but not unambiguously supported by Fig. 4.

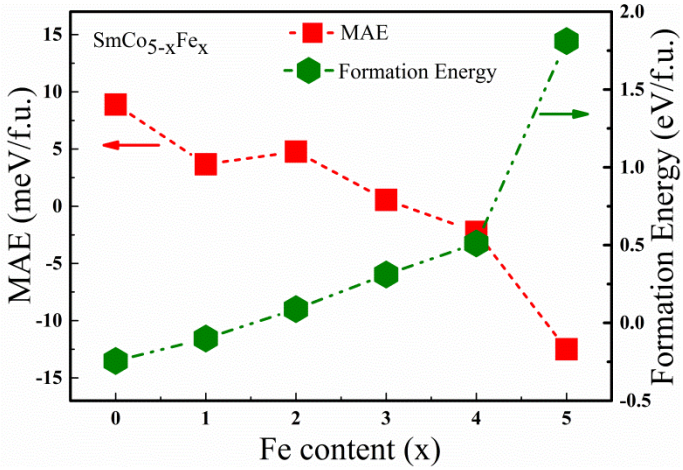

FIG. 5. Theoretically calculated magnetocrystalline anisotropies and formation energies of $SmCo_{5-x}Fe_x$ as a function of Fe content.

Figure 6 plots the total spin moment per formula unit and the Sm orbital moment as a function of Fe content. The calculated Sm orbital moment is antiparallel to the total spin

moment, which is contradictory to the experimental situation in most or all RE-TM intermetallics. In transition-metal-rich RE-TM alloys of late transition metals (such as Fe and Co) and light rare earth elements (such as Sm), the rare-earth orbital moment is parallel, not antiparallel to the TM (and total) spin moment (see e.g. p. 154 in Ref. 46). Furthermore, aside from the sign, the magnitude of Hund's-rules orbital moment of Sm is 5 μ_B, as opposed to 3.5 μ_B or less in the present calculations. The reduced orbital moment indicates that the calculations imply a substantial orbital-moment quenching, thereby violating Hund's second rule, which states that the orbital moment is maximized subject to the first rule (spin maximization). From the viewpoint of total magnetization, the relatively small Sm contribution to the total magnetization contains two striking deviations from Hund's rules behavior that nearly cancel each other: the RE-TM exchange coupling has the wrong sign and the orbital moment is underestimated substantially. This explains why our net magnetization of 9.1 μ_B per f.u. (contribution from total spin and total orbital moments = 11.9 + (-2.8) = 9.1) agrees very well with the experimental value of about 8.5 μ_B [5,17,38]. Figure 6 also predicts a substantial change in the RE orbital moment when going from $SmCo_5$ to $SmFe_5$. We note here that while initializing the calculations, we set up the spin moments of Sm 4*f* and spin moments of Co 3*d* in the same directions. The converged 4*f* orbital moments come out to be negative thereby resulting a net Sm 4*f* moment. The LSDA+U with spin orbit coupling only considers the total angular momentum J = L+S, however, the converged electronic structure results with opposite 4*f* spin and 4*f* orbital moments and with both positive spin and orbital Co 3*d* moments. Furthermore, $SmFe_5$ does not exist and cannot, therefore, be used for comparison with experiment, but many other carefully investigated R_xT_y intermetallics exist for both T = Fe and T = Co, without any trace of TM-induced orbital-moment changes [17,38].

Note that accidental computational errors in the present DFT calculations can safely be excluded. While the accuracy of rare-earth DFT calculations is a matter of debate (see below), our present results are consistent with previous calculations. The 2004 paper by Larson *et al.* [41] uses a fairly different method, but their results show similar trends with respect to the orbital moment (–2.8 μ_B per Sm), although the authors do not emphasize this point in their paper and discuss Hund's first rule only (spin moment).

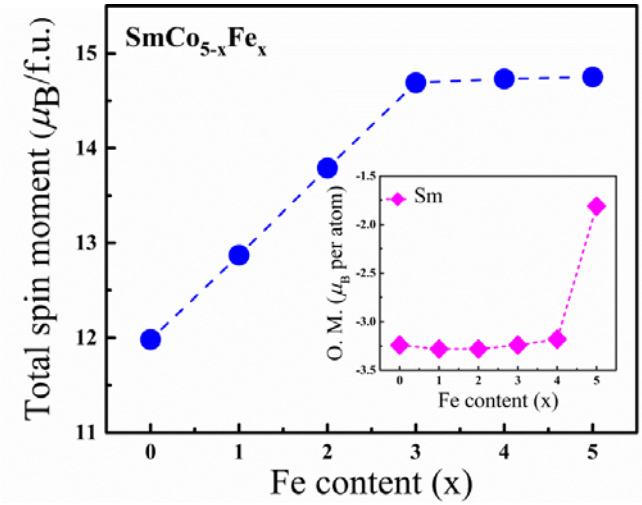

FIG. 6. Total spin moment and orbital moment of Sm-atom (inset figure) of $SmCo_{5-x}Fe_x$ as a function of Fe content. The spin moment is opposite in sign with the Sm-4*f* orbital moment as expected from Hund's rule.

III. ORBITAL MOMENT, CHARGE DENSITY, AND ANISOTROPY

Most RE-TM intermetallics are well-described by a hybrid approach that combines rare-earth crystal-field theory [6,17,38,40,47] with the transition-metal LSDA calculations outlined in the previous paragraphs. For light rare earth elements, such as Sm, the low-temperature RE and TM sublattice moments are parallel due to ferromagnetic net intersublattice coupling. However, the RE 4*f* moment is small, since Hund's third rule yields an antiferromagnetic coupling between the orbital (L) and spin (S) moments. This coupling corresponds to a very complicated intra-atomic spin structure. For example, the $J = 5/2$ Hund's-rules ground state of the Sm^{3+} ion is characterized by the quantum numbers $L = 5$ and $S = 5/2$. Naively subtracting the spin moment ($2S$) from the orbital moment (L) would yield a zero net Sm^{3+} moment ($g = 0$). In fact, the Sm^{3+} ground-state wave function is a superposition of Slater determinants, which reproduces the observed Hund's-rules value of $g = 0.286$. Samarium is also unique in the sense that the first excited multiplet ($J = 7/2$) has energy only about 0.12 eV [47], which corresponds to $g = 0.825$ and somewhat enhances magnetization and anisotropy [17]. Note that this J mixing does not involve a reduction (quenching) of the orbital moment. Concerning magnetocrystalline anisotropy, the Sm atoms in $SmCo_5$ provide about 75% of the room temperature anisotropy, whereas each Co atom per formula unit contributes about 5%. At room temperature, the Sm contribution is approximately 60%.

The two-sublattice approach explains a broad variety of zero- and finite-temperature experimental findings, including for example the temperature dependence of the anisotropy, but is unsatisfactory from the viewpoint of first-principle theory. However, the LSDA+U is not very well equipped to handle strongly correlated electrons, such as 4*f* electrons in Sm, because it considers a single Hartree-Fock-like Slater determinant of pseudo-wave functions [52]. It has been argued that DFT is able to predict the correct ground-state energy of any magnetic system, but the Sm anisotropy involves excited states (J-mixing), and the density functional for combined 3*d*-4*f* systems is not known. In cases where the density functionals for highly correlated systems are known [57, 58], the functionals look actually very different from LSDA(+U) density functionals.

An important Sm-Co-specific question is the degree of orbital-moment quenching. The quenching reflects the chimeric nature of the crystal field (CF). On the one hand, the crystal field realizes magnetocrystalline anisotropy through the spin-orbit coupling $\lambda \boldsymbol{L}\cdot\boldsymbol{S}$. On the other hand, when the crystal field becomes too large, then it suppresses the orbital moment and neutralizes the spin-orbit effect ($\langle \boldsymbol{L}\cdot\boldsymbol{S} \rangle = 0$). In 3*d* systems, including the transition-metal sublattices in RE-TM intermetallics, λ is of the order of 40 meV per atom, much smaller than the crystal field, which is of the order of 1000 meV per atom. These systems are strongly quenched and the anisotropy energy per atom is much smaller than the CF energy, at most a few 0.1 meV per atom. Physically, the 3*d* charge distribution is almost completely determined by the crystal field or, equivalently, by the chemical-bonding strength or band width [60]. In this limit, the spin-orbit coupling yields only minor distortion of the electron charge cloud. The opposite situation is encountered in rare earths. Consider, for example, Sm_2Co_{17}, where the experimental crystal-field splitting is about 2 meV per atom, as compared to the Sm^{3+} SOC of the order of about 150 meV per atom. The strong SOC means that the orbital moment (charge cloud) of the Sm 4*f* electrons is rigidly coupled to the spin by SOC and that the CF creates virtually no deformation of the 4*f*

charge cloud. Rotating the spin merely changes the energy of the Sm^{3+} ion in the crystal field, so that the anisotropy is equal to the electrostatic CF energy of the 4*f* electron cloud.

For $SmCo_5$, the same experimental analysis yields crystal-field energy of about 8 meV per atom. This energy and the corresponding anisotropy constant K_1 are four times bigger than those of Sm_2Co_{17}, making $SmCo_5$ the permanent-magnet material with the highest anisotropy. However, the value of 8 meV remains much smaller than 150 meV, so the degree of quenching should be very low, in contrast to our present calculations, where the CF energy is comparable to or larger than 150 meV per atom.

This paradox puts Sm-Co research into a completely new light: generations of rare-earth researchers have made a gigantic mistake in the evaluation of experimental data, or are LSDA+*U* estimates of the crystal field wrong by more than an order of magnitude? We will not be able to answer this question here, and we actually believe that a thorough understanding of electron correlations in RE-TM intermetallics will be a challenge to future research. However, a more detailed analysis of the problem is in order.

Figure 7 illustrates the difference between traditional crystal-field theory (a-b) and crystal-field theory with partial quenching (c-d); the big arrows show the direction of the rare-earth spin. The charge distribution of Hund's-rules rare-earth ions, prolate or 'cigar-shaped' in the case of Sm^{3+}, is given by the Stevens coefficients α_J, β_J, and γ_J [6,59]. The large spin-orbit coupling of the Sm 4*f* electrons means that the rare-earth spin is rigidly coupled to the orbital moment, that is, to the charge distribution $\rho(\boldsymbol{r})$ of the 4*f* electrons [40]. The crystal field can be modeled by assigning crystal-field charges to the surrounding Co atoms or 'ligands', and experiment shows that these effective charges are almost always negative, very light atoms (H, B) being possible exceptions [61]. Since the negatively charged ends of the prolate Sm^{3+} 4*f* electron distribution and the negative crystal field charges repel each other electrostatically, the configuration (a) is energetically more favorable than (b). This repulsion is the origin of the strong easy-axis anisotropy of $SmCo_5$ and other RE-TM intermetallics.

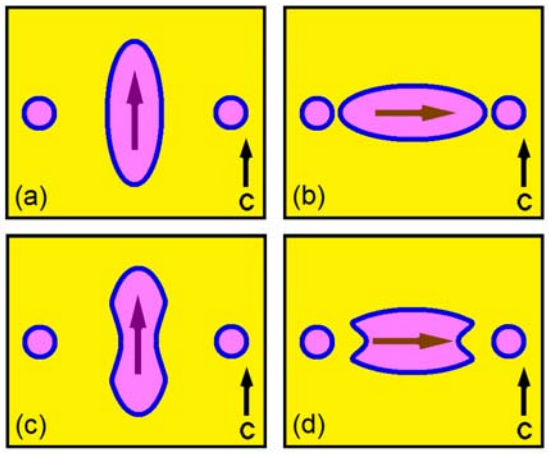

FIG. 7. Quenching, charge distribution, and anisotropy (schematic): (a) charge distribution in terms of Stevens coefficients, (b) rare-earth moment in the hard direction, (c) effect of crystal field on the charge distribution for the easy direction, and (d) effect of crystal field on the charge distribution in a hard direction. Bluish regions denote the negative charges of the Sm^{3+} ion (center) and of the Co 'ligands' (small circles).

In the idealized limit of Figs. 7(a-b), the crystal-field interaction (about 10 meV) is too weak to compete against the spin-orbit coupling (about 150 meV) and leaves the shape of the 4f charge cloud unchanged. As far as the 4f wave functions are concerned, this limit corresponds to zeroth-order perturbation theory. In higher-order perturbation theory, the crystal-field distorts the shape of the 4f electron cloud, as shown in Figs. 7(c-d). Explicit calculations of type (c) have been performed by Walter [62]. The deformation of the charge cloud corresponds to orbital-moment quenching [6,40] and means that the anisotropy-energy difference between (c) and (d) is smaller than that between (a) and (b). In the 3*d* limit (crystal field and/or interatomic hopping energies much higher than SOC), the charge density is only weakly disturbed by the SOC and the anisotropy is low.

While the anisotropy mechanism outlined in Fig. 7 remains qualitatively valid on a DFT level, the actual calculations behind Figs. 7(a-c) are semiquantitative, based on point-charge-type crystal-field parameters. Furthermore, no attempts have been made up until now to explicitly calculate the energy and charge-density differences between the configurations (c) and (d), that is, between rare-earth spins $\boldsymbol{S}$ pointing in the *c*- and *a*- or *b*-directions. If the basic picture of Fig. 7 is correct, then the change from Fig. 7(a-b) to Fig. 7(c-d) should be recognizable in density-functional calculations of the electron charge density $\rho(\boldsymbol{r})$, irrespective of the accuracy of the used method.

Figure 8 shows the calculated total charge density obtained by LSDA+*U*. The Sm atom is located in the centers of (a) and (b), and the magnetization is along with the *c*-axis (a) and in the *a*-*b*-basal plane (b). Both the spin-orbit coupling and the crystal-field interaction are much smaller than the total band width, but the differences in the shape of the rare-earth charge distribution are nevertheless clearly visible. In the LSDA (including LSDA+*U*), the pseudo wave functions used to construct $\rho(\boldsymbol{r})$ are delocalized, that is, periodically repeated in space due to interatomic hopping. This should never happen with Hund's-rules ions, and the corresponding overestimation of interatomic hopping amounts to overestimating quenching. The plus-*U* approximation semi quantitatively corrects this error by creating a Hubbard-like spin splitting of the 4*f* electrons, which suppresses interatomic hopping and the corresponding unphysical 4*f* charge fluctuations. However, Hund's-rules many-electron interactions are likely to further reduce hopping and quenching without invalidating the charge- and Hubbard-splitting-related benefits of the LSDA+*U*.

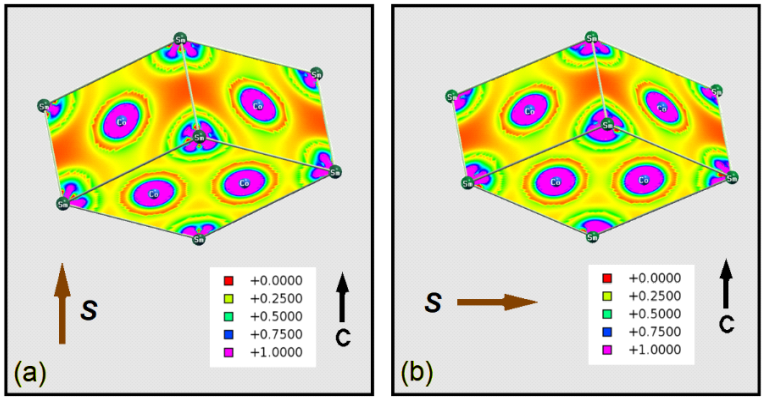

FIG. 8. The charge density ρ as calculated by DFT: (a) easy direction and (b) hard direction. The charge density has ranged from 0 to 1 e/Å^3.

While the accuracy of anisotropy constants and orbital moments obtained by LSDA+*U* is in need of further debate, the basic charge-density picture elaborated in Fig 8 is likely to survive future scrutiny. Many-electron calculations of K_1 and $\rho(\boldsymbol{r}, \boldsymbol{S})$ should include correlations beyond the plus-*U* approximation, which is a challenge to research in the medium and far future.

IV. CONCLUSIONS

In summary, we have used experiment and theory to investigate the structural and magnetic properties of melt-spun $SmCo_{5-x}Fe_x$ ($0 \leq x \leq 2$). Many features of the system are consistent with past research, but some of the theoretical findings are seemingly contradictory to past research. The disagreement is not caused by numerical errors or accidental mistakes but reflects how the many-electron nature of the rare-earth 4*f* electrons is interpreted by crystal-field and LSDA+*U* theories. The two-sublattice crystal-field theory is known to describe a broad variety of Sm-Co properties, such as the temperature dependence of magnetization and anisotropy, but it is not a first-principle approach. By contrast, our first-principle approach, LSDA+*U*, yields a substantial orbital-moment quenching, which violates Hund's rules and is contradictory to conventional knowledge accumulated over several decades of rare-earth research. Rationalizing the orbital-moment quenching in terms of the dependence of the 4*f* charge distribution on the magnetization angle, we argue that medium- and long-run future research will be necessary to reconcile experiment, sublattice models, and first-principle calculations.

Acknowledgment

This work is supported by the Critical Materials Institute, an Energy Innovation Hub funded by the U.S. Department of Energy, Office of Energy Efficiency and Renewable Energy, Advanced Manufacturing Office. The Ames Laboratory is operated for the U.S. Department of Energy by Iowa State University of Science and Technology under contract No. DE-AC02-07CH11358. R. C. and D. P. would like to acknowledge Ed Moxley for maintaining and updating computational facilities and software packages including the Raman cluster and the Wien2k program. The work in Nebraska was supported by the US Department of Energy (Grant No. DE-FG02-04ER46152) and performed in part in the Nebraska Nanoscale Facility and the Nebraska Center for Materials and Nanoscience which are supported by NSF NNCI #1542182, and the Nebraska Research Initiative. Thanks are due to J. E. Shield and S. R. Valloppilly for assistance and helpful discussions.

References

[1] K. Strnat, G. Hoffer, J. Olson, W. Ostertag, and J. J. Becker, A Family of New Cobalt□Base Permanent Magnet Materials, Journal of Applied Physics **38**, 1001 (1967).

[2] K. Strnat, Legierungen des Kobalts mit Seltenerd-Metallen, eine neue Gruppe aussichtsreicher Dauermagnetwerkstoffe, Z. Kobalt **36**, 119-128 (1967).

[3] K. J. Strnat, Rare-Earth Magnets in Present Production and Development, J. Magn. Magn. Mater. **7**, 351-360 (1978).

[4] K. J. Strnat and R. M. W. Strnat, Rare earth-cobalt permanent magnets, J. Magn. Magn. Mater. **100**, 38-56 (1991).

[5] K. Kumar, $RETM_5$ and RE_2TM_{17} permanent magnets development, J. Appl. Phys. **63**, R13-57 (1988).

[6] R. Skomski and J. M. D. Coey, *Permanent Magnetism*, Institute of Physics, Bristol 1999.

[7] R. Skomski, Nanomagnetics, J. Phys.: Condens. Matter **15**, R841-896 (2003).

[8] O. Gutfleisch, M. A. Willard, E. Brück, C. H. Chen, S. G. Sankar, and J. P. Liu, Magnetic materials and devices for the 21st century: stronger, lighter, and more energy efficient, Adv. Mater. **23**, 821 (2011).

[9] R. Skomski, P. Manchanda, P. Kumar, B. Balamurugan, A. Kashyap, and D. J. Sellmyer, Predicting the Future of Permanent-Magnet Materials (invited), IEEE Trans. Magn. **49** (7) 3215-3220 (2013).

[10] K. H. J., Buschow, P. A., Naastepad, and F. F. Westendorp, Preparation of $SmCo_5$ Permanent Magnets, J. Appl. Phys. **40**, 4029–4032 (1969).

[11] M. H. Walmer, J. F. Liu, and P. C. Dent, Current Status of permanent-Magnet Industry in the United States, in Rare Earth Permanent Magnets and their Applications, Ed. D. Niarchos (Admore Press, Athens, 2008), p. 37-41.

[12] A. M. Duerrschnabel, M. Yi, K. Uestuener, M. Liesegang, M. Katter, H.-J. Kleebe, B. Xu, O. Gutfleisch, and L. Molina-Luna, Atomic structure and domain wall pinning in samarium-cobalt-based permanent magnets, Nat. Commun. **8**, 54 (2017).

[13] K. Strnat, The recent development of permanent magnet materials containing rare earth metals, IEEE Trans. Magn. **6** (2), 182–190 (1970).

[14] J. M. D. Coey, Hard Magnetic Materials: A Perspective, IEEE Trans. Magn. **49**, 4671-4681 (2011).

[15] J. J. M. Franse, N. P. Thuy, and N. M. Homg, Individual site magnetic anisotropy of the iron and cobalt ions in rare earth-iron and rare earth-cobalt intermetallic compounds, J. Magn. Magn. Mat. **72**, 361-366 (1988).

[16] A. E. Ray and K. Strnat, Easy Directions of Magnetization in Ternary $R_2(Co, Fe)_{17}$ Phases, IEEE Trans. Magn. **8**, 516-518 (1972).

[17] K. H. J. Buschow, Intermetallic compounds of rare-earth and 3*d* transition metals, Rep. Prog. Phys. **40**, 1179-1256 (1977).

[18] C. H. Chen, S. Kodat, M. H. Walmer, Sh.-F. Cheng, M. A. Willard, and V. G. Harris, Magnetic and Structural Properties of $Sm(Co_{1-x}Fe_x)_z$ Based Powders and Spin Cast Ribbons, Eds. G. C. Hadjipanayis and M. J. Bonder, Rinton Press, Princeton 2002, p. 844-852.

[19] J. Zhou, R. Skomski, C. Chen, G. C. Hadjipanayis, and D. J. Sellmyer, Sm-Co-Ti High-temperature permanent magnets, Appl. Phys. Lett. **77**, 1514-1516 (2000).

[20] J. C. Tellez-Blanco, R. Grossinger, and R. S. Turtelli, Structure and magnetic properties of $SmCo_{5-x}Cu_x$ alloys, J. Alloys Compd. **281**, 1-5 (1998).

[21] R. F. Sabirianov, A. Kashyap, R. Skomski, S. S. Jaswal, and D. J. Sellmyer, First-principles study of transition-metal substitutions in Sm-Co permanent magnets, Appl. Phys. Lett. **85**, 12 (2004).

[22] A. Laslo, C. V. Colin, O. Isnard, and M. Guillot, Effect of the M/Co substitution on magnetocrystalline anisotropy and magnetization in $SmCo_{5-x}M_x$ compounds (M=Ga; Al), J. Appl. Phys. **107**, 09A732 (2010).

[23] H. Zaigham and F. Ahmad Khalid, Exchange Coupling and Magnetic Behavior of $SmCo_{5-x}Sn_x$ Alloys, J. Mater. Sci. Technol. **27**, 3 (2011).

[24] S. Q. Yin, H. Wang, H. B. Zhao, Y. Jiang, and J. P. Wang, The effects of Cu doping on crystalline structure and magnetic properties of $SmCo_{5-x}Cu_x$ thin films grown on Ru (0002), J. Appl. Phys. **114**, 213908 (2013).

[25] T. Saito and D. Nishio-Hamane, Magnetic properties of $SmCo_{5-x}Fe_x$ (x = 0–4) melt-spun ribbon, J. Alloys Compd. **585**, 423-427 (2014).

[26] P. Soderlind, A. Landa, I. L. M. Locht, D. Aberg, Y. Kvashnin, M. Pereiro, M. Dane, P. E. A. Turchi, V. P. Antropov, and O. Eriksson, Prediction of the new efficient permanent magnet $SmCoNiFe_3$, Phys. Rev. B **96**, 100404 (2017); and, A. Landa, P. Soderlind, D. Parker, D. Aberg, V. Lordi, A. Perron, P. E. A. Turchi, R. K. Chouhan, D. Paudyal and T. A. Lograsso, Thermodynamics of $SmCo_5$ compound doped with Fe and Ni: An *ab initio* study, J. Alloys Compd. **765**, 659 (2018).

[27] A. J. Perry and A. Menth, Permanent Magnets Based on $Sm(Co, Cu, Fe)_z$, IEEE Trans. Magn. **11** (5), 1423-1425 (1975).

[28] J. Fidler and P. Skalicky, Microstructure of precipitation hardened cobalt rare earth permanent magnets, J. Magn. Magn. Mater. **27**, 127 (1982).

[29] M. Katter, J. Weber, W. Assmus, P. Schrey, and W. Rodewald, A New Model for the Coercivity Mechanism of $Sm_2(Co, Fe, Cu, Zr)_{17}$ Magnets, IEEE Trans. Magn. **32** (5), 4815-4817 (1996).

[30] L. Steinbeck, M. Richter, U. Nitzsche, and H. Eschrig, Ab initio calculation of electronic structure, crystal field, and intrinsic magnetic properties of Sm_2Fe_{17}, $Sm_2Fe_{17}N_3$, $Sm_2Fe_{17}C_3$, and Sm_2Co_{17}, Phys. Rev. B **53**, 7111 - 7127 (1996).

[31] R. Skomski, Domain-wall curvature, and coercivity in pinning-type Sm-Co magnets, J. Appl. Phys. **81** (1997) 5627-5629.

[32] M. Katter, Coercivity calculation of $Sm_2(Co, Fe, Cu, Zr)_{17}$ magnets, J. Appl. Phys. **83**, 6721-6723 (1998).

[33] B. Streibl, J. Fidler, and T. Schrefl, Domain Wall Pinning in High-Temperature Sm(Co, Fe, Cu, $Zr)_{7-8}$ Magnets, J. Appl. Phys. **87**, (2000) 4765-4767.

[34] W. Scholz, J. Fidler, T. Schrefl, D. Suess, and T. Matthias, Micromagnetic three-dimensional simulation of the pinning field in high-temperature $Sm(Co, Fe, Cu, Zr)_z$ magnets, J. Appl. Phys. **91**, 8492-1-3 (2002).

[35] T. Miyazaki, M. Takahashi, X. Yang, H. Saito, and M. Takahashi, Formation of metastable compounds and magnetic properties in rapidly quenched $(Fe_{1-x}Co_x)_5Sm$ and $(Fe_{1-x}Co_x)_7Sm_2$ alloy systems, J. Appl. Phys. **64**, 5974-5976 (1988).

[36] T. Miyazaki, M. Takahashi, X. Yang, H. Saito, and Takahashi, Formation and magnetic properties of metastable $(TM)_5Sm$ and $(TM)_7Sm_2$ (*TM* = Fe, Co) compounds, J. Magn. Magn. Mater. **75**, 123-129 (1988).

[37] K. H. J. Buschow, A. M. van Diepen, and H. W. de Wijn, Crystal-field anisotropy of Sm^{3+} in $SmCo_5$, Solid State Commun. **15**, 903-906 (1974).

[38] H. R. Kirchmayr and C. A. Poldy, Magnetism in Rare Earth-3*d* Intermetallics, J. Magn. Magn. Mater. **8**, 1-42 (1978).

[39] S. G. Sankar, V. U. S. Rao, E. Segal, W. E. Wallace, W. G. D. Frederick, and H. J. Garrett, Magnetocrystalline anisotropy of $SmCo_5$ and its interpretation on a crystal-field model, Phys. Rev. B **11**, 435-439 (1975).

[40] R. Skomski, *Simple Models of Magnetism*, University Press, Oxford (2008).

[41] P. Larson, I. I. Mazin, and D. A. Papaconstantopoulos, Effects of doping on the magnetic anisotropy energy in $SmCo_{5-x}Fe_x$ and $YCo_{5-x}Fe_x$, Phys. Rev. B **69**, 134408 (2004).

[42] M. Richter, Band structure theory of magnetism in 3d-4f compounds, J. Phys. D: Appl. Phys. **31**, 1017-1048 (1998).

[43] R. Coehoorn, Calculated electronic structure and magnetic properties of Y-Fe compounds, Phys. Rev. B **39**, 13072 (1989).

[44] D. Givord, J. Laforest, H. S. Li, A. Liénard, R. De La Bâthie, and P. Tenaud, Rare Earth-Transition Metal Permanent Magnets, Journal de Physique Colloques **46**, C6-213-220 (1985).

[45] N. H. Duc, T. D. Hien, D. Givord, J. J. M. Franse, and F. R. de Boer, Exchange interactions in rare-earth transition-metal compounds, J. Magn. Magn. Mater. **124** (1993) 305-311.

[46] J. M. D. Coey, *Magnetism and Magnetic Materials* (Cambridge University Press, 2010).

[47] K. N. R. Taylor and M. I. Darby, Physics of Rare Earth Solids, Chapman and Hall, London 1972.

[48] P. Larson and I. I. Mazin, Magnetic properties of $SmCo_5$ and YCo_5, J. Appl. Phys. **93**, 6888-90 (2003).

[49] J. F. Herbst, $R_2Fe_{14}B$ materials: Intrinsic properties and technological aspects, Rev. Mod. Phys. **63** (1991) 819-898.

[50] N. W. Ashcroft and N. D. Mermin, *Solid State Physics*, Saunders, Philadelphia 1976.

[51] P. Fulde, *Electron Correlations in Molecules and Solids*, Springer, Berlin 1991.

[52] A. Avella and F. Manchini (Eds.), *Strongly Correlated Systems: Theoretical Methods*, Springer, Berlin 2012.

[53] P. Soderlind, P. E. A. Turchi, A. Landa and V. Lordi, Ground-state properties of rare-earth metals: an evaluation of density-functional theory, J. Phys.: Condens. Matter **26**, 416001 (2014).

[54] B. D. Culltiy, Elements of X-Ray Diffraction, Pearson (2001).

[55] P. Scherrer, Estimation of the size and internal structure of colloidal particles by means of röntgen, Nachr Ges Wiss Gottingen **96**, 96-100 (1918).

[56] A. L. Patterson, The Scherrer formula for X-ray particle size determination, Phys. Rev. **56**, 978-82 (1939).

[57] E. Runge and G. Zwicknagl, Electronic structure calculations and strong correlations: a model study, Ann. Physik **5**, 333-354 (1996).

[58] R. Skomski, P. Manchanda, and A. Kashyap, Correlations in rare-earth transition-metal permanent magnets, J. Appl. Phys. **117**, 17C740-1-4 (2015).

[59] C. J. Ballhausen, *Ligand field theory*, McGraw-Hill, New York 1962.

[60] M. T. Hutchings, Point-charge calculations of energy levels of magnetic ions in crystalline electric fields, Solid State Phys. **16**, 227-273 (1964).

[61] D. J. Newman and B. Ng, The superposition model of crystal fields, Rep. Prog. Phys. **52**, 699-763 (1989).

[62] U. Walter, Charge distributions of crystal field states, Z. Phys. B **62**, 299-309 (1986).